Multilevel Robust State Observer for Spatial Alumina Concentration Estimation

Luning Ma[1], Choon-Jie Wong[2], Jie Bao[3], Maria Skyllas-Kazacos[4], Barry Welch[5], Jing Shi[6] and Mohamed Mahmoud[7]
1. PhD student
2. Postdoctoral Research fellow
3, 4, 5. Professor
School of Chemical Engineering, The University of New South Wales, Sydney, Australia
6. Lead Engineer, Research and Development
7. Manager, Centre of Excellence
Emirates Global Aluminium (EGA), Dubai, United Arab Emirates
Corresponding author: j.bao@unsw.edu.au
https://doi.org/10.71659/icsoba2024-al019

Abstract

In the aluminium smelting process, the information on spatial variations in alumina concentration is crucial for online alumina feeding control. However, the harsh environment of smelting cells renders long-term continuous real-time measurement of alumina concentrations impractical. Model-based state observers can be utilised for real-time estimation of the spatially distributed alumina concentrations, but the challenge lies in addressing model uncertainties, such as those in bath flow velocities and anode-cathode distance. To address these challenges, an H_∞ filter-based multilevel state observer is proposed for estimating spatial alumina concentration. This method can estimate alumina concentrations within a reasonable range and is robust to uncertainties. The effectiveness of this method is validated through experimental studies.

Keywords: Aluminium electrolysis, Process monitoring, State observer.

1. Introduction

In the aluminium smelting process, the control of alumina concentration plays an important role in improving the process efficiency. Inappropriate control can lead to various abnormal conditions, such as anode effects or sludge formation [1-6]. The existing alumina feed control algorithm employs a kind of logic control, which includes different feed windows [7]. To improve the control accuracy of alumina concentrations, reliable information of alumina concentration under different cell conditions is required. Traditional methods for getting alumina concentration information rely on periodic sampling and laboratory analysis, which can be time-consuming [2]. Therefore, online monitoring is necessary to improve the control of alumina concentrations.

The commonly used method for process monitoring is the extended Kalman filter (EKF), and many researchers have applied it in the aluminium smelting process. Shi [7,8] used the EKF to estimate average alumina concentration and utilised the results for control investigations. Yao [10] applied the EKF to investigate average alumina concentration and corresponding dissolution rate. However, since the EKF is designed to minimise the mean-squared error under the assumption of Gaussian noise, it may provide inaccurate estimations when abnormal cell conditions, such as anode effect, occur due to increased noise uncertainty. In contrast, the H_∞ filter can minimise the estimation error in the worst-case scenario [11]. Rao [12] compared the Kalman filter and H_∞ filter, and the results showed that the H_∞ filter can have a better estimation performance under worst-case noise conditions. Poveda [13] also conducted a comparison and concluded that H_∞ filter converges faster than the Kalman filter under additive noise. Therefore,

in the aluminium smelting process, H_∞ filter is more robust for the estimation of alumina concentration.

On the other hand, online estimation struggles with variability of alumina distribution due to limitations in spatial information. Based on the aluminium electrolysis mechanism, the localised consumption of alumina is related to the individual anode currents. With spatial information from individual anode current measurements, the distribution of alumina concentrations can be estimated [14]. Additionally, the localised alumina concentrations are also affected by the bath flow patterns, which are difficult to obtain and introduce additional uncertainties into the process system [15]. To address these challenges, an H_∞ filter based multilevel state observer utilising individual anode current measurements is proposed for online estimation of the spatial alumina concentration. By using the data provided by individual anode currents, this method can enhance the spatial resolution and accuracy of spatial alumina concentration estimations.

In this paper, the structure is organised as follows: the process model is first introduced. Then, the design of an H_∞ filter is described. Following that, the structure of multilevel state observer is introduced. Finally, the effectiveness of this method is validated through experimental studies.

2. Process Modelling of Aluminium Smelting Process

The Hall-Héroult process is the commonly applied method for producing alumina in industry. In this process, the dumped alumina dissolves into the molten cryolite and is electrolysed into aluminium. The overall reaction in the aluminium smelting process can be simply represented as follows:

$$2Al_2O_3 + 3C \rightarrow 4Al(l) + 3CO_2(g) \quad (1)$$

$$Al_2O_3 + 3C \rightarrow 2Al(l) + 3CO(g) \quad (2)$$

where the ratio of CO_2:CO in the product is typically in the range between 5 and 10 [12].

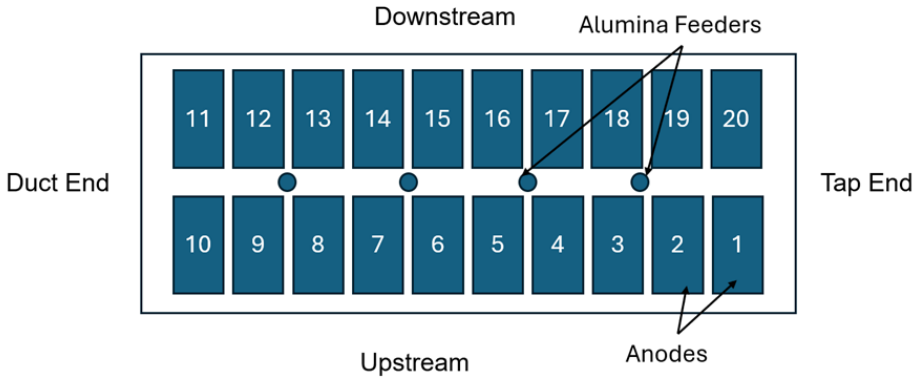

Figure 1. Layout of the anodes.

For an aluminium cell with 20 anodes and 4 alumina feeders, as shown in Figure 1, for a 1-minute time step, the dynamics of alumina concentration can be described by the following process model [15]:

$$C_{Al_2O_3,slow,k+1} = C_{Al_2O_3,slow,k} + t_s\left(-k_{slow}C_{Al_2O_3,slow,k} + \frac{P_{Al_2O_3}m_{feed,k}(1-r)}{m_{bath}}\right) \quad (3)$$

$$C_{Al_2O_3,d,k+1} = C_{Al_2O_3,d,k} + t_s\left(\frac{P_{Al_2O_3}m_{feed,k}}{m_{bath}}r + k_{slow}C_{Al_2O_3,slow,k} - \frac{Fa(I_k)}{m_{bath}}\right) \quad (4)$$

$$ACD_{k+1} = ACD_k + t_s(-\delta_{metal\ accum} + \delta_{anode\ consum}) + b_{m,k} \quad (5)$$

where:

$C_{Al_2O_3,slow,k}$	Concentration of undissolved alumina which can dissolve slowly at the k-th time, %wt
t_s	Sampling interval, s
k_{slow}	Slow dissolution rate, s^{-1}
$P_{Al_2O_3}$	Purity of alumina feed, %
$m_{feed,k}$	Alumina feed at the k-th time, kg/s
$C_{Al_2O_3,d,k}$	Concentration of dissolved alumina, %wt
ACD_k	Anode-Cathode distance at the k-th time, m
$\delta_{metal\ accum}$	Metal accumulation rate, m/s
$\delta_{anode\ consum}$	Anode consumption rate, m/s
$b_{m,k}$	Beam movement at the k-th time, m
r	Fraction of undissolved alumina which can dissolve quickly
$V_{cell,k}$	Cell voltage at the k-th time, V
I_k	Line current at the k-th time, A

For the specific alumina concentration and ACD, the corresponding cell voltage can be described as follows [15]:

$$V_{cell} = \mathrm{E_{ca}} + E_{sa} + E_{cc} + E_{rev} + I_{line}(R_{an} + R_{bub} + R_{bath} + R_{ca}) + V_{external} \quad (6)$$

where:

$\mathrm{E_{ca}}$	Concentration overvoltage at the anode, V
E_{sa}	Surface overvoltage at the anode, V
E_{cc}	Concentration overvoltage at the cathode, V
E_{rev}	Reversible potential, V
R_{an}	Anode resistance, Ω
R_{bub}	Bubble layer resistance, Ω
R_{bath}	Bath resistance, Ω
R_{ca}	Cathode resistance, Ω
$V_{external}$	External voltage drop from cell to cell, V
I_{line}	Line current, A

To describe the process concisely, the above system equations ((3) – (6)) can be rewritten by the following equations:

$$x_{k+1} = f(x_k, u_k, w_k) \quad (7)$$

$$y_{k+1} = h(x_{k+1}, v_{k+1}) \quad (8)$$

where:

system states $x_k = \left[C_{Al_2O_3,slow,k}, C_{Al_2O_3,d,k}, ACD_k\right]^T$

system output $y_k = V_{cell,k}$

system control input: $u_k = \left[I_k, m_{feed,k}, b_{m,k}\right]^T$

w_k	Process noises at the k-th time
v_k	Measurement noises at the k-th time

3. Design of the H_∞ Filter

Based on the established model in Section 2, the main mass dynamics of this process can be captured, but there are still mismatches between the model and the real process. To minimise the effect of model uncertainty on the estimation, a robust state observer is required. Therefore, the design of an H_∞ filter is proposed in this section for the estimation of an average alumina concentration.

For the design of an H_∞ filter, the cost function is given as follows:

$$J = \frac{\sum_{k=0}^{N-1} \|x_k - \hat{x}_k\|}{\|x_0 - \hat{x}_0\|^2_{P_0^{-1}} + \sum_{k=0}^{N-1} \left(\|w_k\|^2_{Q^{-1}} + \|v_k\|^2_{R^{-1}} \right)} \tag{9}$$

where:

P_0 Square matrix of the initial estimation error
Q Noise weighting of process noises
R Nosie weighting of measurement noises

Following the cost function, the detailed strategy can be designed as described in [11]:

$$K_k = P_k \left[I - \theta P_k + H_k^T R^{-1} H_k P_k \right]^{-1} H_k^T R^{-1} \tag{10}$$

$$\hat{x}_{k+1} = F_k \hat{x}_k + F_k K_k (y_k - H_k \hat{x}_k) \tag{11}$$

$$P_{k+1} = F_k P_k \left[I - \theta P_k + H_k^T R^{-1} H_k P_k \right]^{-1} F_k^T + Q_k \tag{12}$$

where:

K_k Correction gain of the H_∞ filter at the k-th time
$\hat{x}_k$ Estimated system state at the k-th time
I Identity matrix
F_k Jacobian matrix of state equation with respect to states at the k-th time
H_k Jacobian matrix of output equation with respect to states at the k-th time
θ $1/\theta$ represents the performance bound of the above cost function

Noted that the following inequality must hold during the running period of the state observer, otherwise the solution will be infeasible.

$$P_k^{-1} - \theta + H_k^T R_k^{-1} H_k > 0 \tag{13}$$

4. Design of the Multilevel State Observer

The multilevel state observer is proposed for estimating spatial alumina concentrations. The implementation of the estimation is performed level by level, as shown in Figure 2. Starting from Level 1, the smelting cell is regarded as a single zone, where the estimation is an average alumina concentration. At Level 2, the smelting cell is treated as two zones. Here, not only are the individual anode currents in each zone considered for spatial estimation, but the estimated results from Level 1 are also used as a soft constraint to make the estimation reasonable. Similarly, the estimated results from Level 2 will be the soft constraint of Level 3. In this paper, there are four alumina feeders in this smelting cell, therefore the dividing process ends at Level 3 with four divided zones, one around each feeder.

Combining the process model in Section 2, the system equations at Level 1 are as follows:

$$x_{L1,,k+1} = f\left(x_{L1,k}, u_{L1,k}, w_{L1,k}\right) \tag{14}$$

$$V_{L1,k+1} = h(x_{L1,k+1}, v_{L1,k+1}) \tag{15}$$

where:

$L1$ Represents variables in Level 1

At level 2, the subsystem in zone 1 and zone 2 can be respectively represented as:

$$x_{L2,z1,k+1} = f\left(x_{L2,z1,k}, u_{L2,z1,k}, w_{L2,z1,k}\right) \tag{16}$$

$$V_{L2,z1,k+1} = h(x_{L2,z1,k+1}, v_{L2,z1,k+1}) \tag{17}$$

and

$$x_{L2,z2,k+1} = f\left(x_{L2,z2,k}, u_{L2,z2,k}, w_{L2,z2,k}\right) \tag{18}$$

$$V_{L2,z2,k+1} = h(x_{L2,z2,k+1}, v_{L2,z2,k+1}) \tag{19}$$

where:

$L2$ Represents variables in Level 2

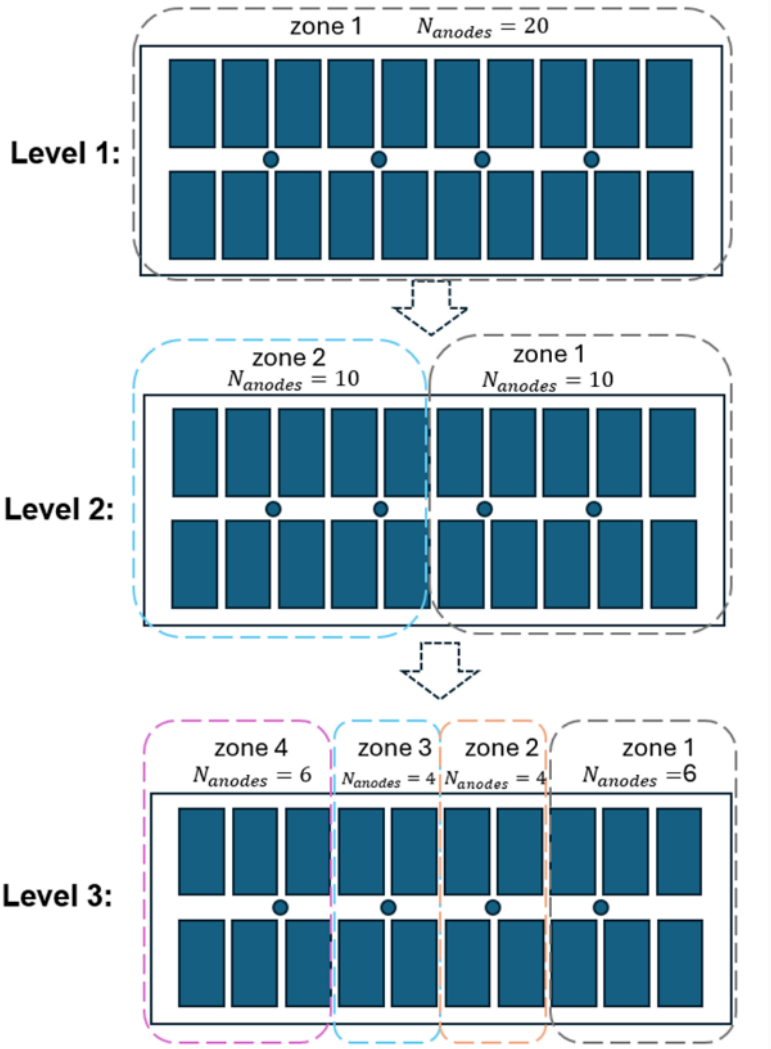

Figure 2. Implementation sequence of multilevel state observer.

Noted that in $u_{L2,i,k}$, the line current is replaced by the sum of anode currents in the specific zone. Additionally, since the average values of alumina concentrations in Leve 2 should be related to the estimation of Level 1, therefore, two additional output equations can be obtained:

$$\hat{C}_{Al_2O_3,d,L1,k} = \frac{(C_{Al_2O_3,d,L2,z1,k} \times m_{bath,L2,z1} + C_{Al_2O_3,d,L2,z1,k} \times m_{bath,L2,z2})}{m_{bath,L2,z1} + m_{bath,L2,z2}} \tag{20}$$

$$\widehat{ACD}_{L1,k} = \frac{ACD_{L2,k} \times N_{anodes,L2,z1} + ACD_{L2,k} \times N_{anodes,L2,z2}}{N_{anodes,L2,z1} + N_{anodes,L2,z2}} \tag{21}$$

where:

$m_{bath,L2,i}$ Bath mass of zone i $(i = 1,2)$ in level 2, kg

$N_{anodes,L2,i}$ Number of anodes in zone i $(i = 1,2)$ in level 2

$\hat{C}_{Al_2O_3,d,L1}$ Calculated alumina concentration of Level 1 based on the estimation results of Level 2, %wt

$\widehat{ACD}_{L1,k}$ Calculated ACD of Level 1 based on the estimation results of Level 2, m

Similarly, the subsystem in Level 3 can be represented by the following subsystem equations:

$$x_{L3,i,k+1} = f(x_{L3,i,k}, u_{L3,i,k}, w_{L3,i,k}) \quad (22)$$

$$V_{L3,i,k+1} = h(x_{L3,i,k+1}, v_{L3,i,k+1}) \quad (23)$$

where:

$L3$ Represents variables in Level 3

i Its value is zone 1, zone 2, zone 3 and zone 4, respectively.

The corresponding additional output equations for Level 3 are:

$$\hat{C}_{Al_2O_3,d,L2,z1,k} = \frac{(C_{Al_2O_3,d,L3,z1,k} \times m_{bath,L3,z1} + C_{Al_2O_3,d,L3,z2,k} \times m_{bath,L3,z2})}{m_{bath,L3,z1} + m_{bath,L3,z2}} \quad (24)$$

$$\widehat{ACD}_{L2,z1,k} = \frac{ACD_{L3,z1,k} \times N_{anodes,L3,z1} + ACD_{L3,z2,k} \times N_{anodes,L3,z2}}{N_{anodes,L3,z1} + N_{anodes,L3,z2}} \quad (25)$$

$$\hat{C}_{Al_2O_3,d,L2,z2,k} = \frac{(C_{Al_2O_3,d,L3,z3,k} \times m_{bath,L3,z3} + C_{Al_2O_3,d,L3,z3,k} \times m_{bath,L3,z3})}{m_{bath,L3,z3} + m_{bath,L3,z4}} \quad (26)$$

$$\widehat{ACD}_{L2,z2,k} = \frac{ACD_{L3,z3,k} \times N_{anodes,L3,z3} + ACD_{L3,z4,k} \times N_{anodes,L3,z4}}{N_{anodes,L3,z3} + N_{anodes,L3,z4}} \quad (27)$$

where:

$m_{bath,L3,i}$ Bath mass of zone i ($i = 1, 2, 3, 4$) in level 3, kg

$N_{anodes,L3,z1}$ Number of anodes in zone i ($i = 1, 2, 3, 4$) in level 3

$\hat{C}_{Al_2O_3,d,L2,z1}$ Calculated alumina concentration of Zone 1 in Level 2 based on the estimation results of Zone 1 and Zone 2 in Level 3, %wt

$\hat{C}_{Al_2O_3,d,L2,z2}$ Calculated alumina concentration of Zone 2 in Level 2 based on the estimation results of Zone 3 and Zone 4 in Level 3, %wt

$\widehat{ACD}_{L2,z1}$ Calculated ACD of Zone 1 in Level 2 based on the estimation results of Zone 1 and Zone 2 in Level 3, m

$\widehat{ACD}_{L2,z2}$ Calculated ACD of Zone 2 in Level 1 based on the estimation results of Zone 3 and Zone 4 in Level 3, m

Therefore, all system equations of each zone in each level have been obtained. Based on the above H_∞ filter proposed in Section 3, the spatial alumina concentrations can be achieved level by level.

5. Experimental Studies

To test the effectiveness of the proposed multilevel state observer, one experiment was conducted. During the experiment, the line current, individual anode currents, alumina feeding rate, beam movements, and cell voltage were recorded at an interval of 1 second. Bath samples from four locations (as shown in Figure 3) were collected and analysed, with a sampling interval of approximately 30 minutes.

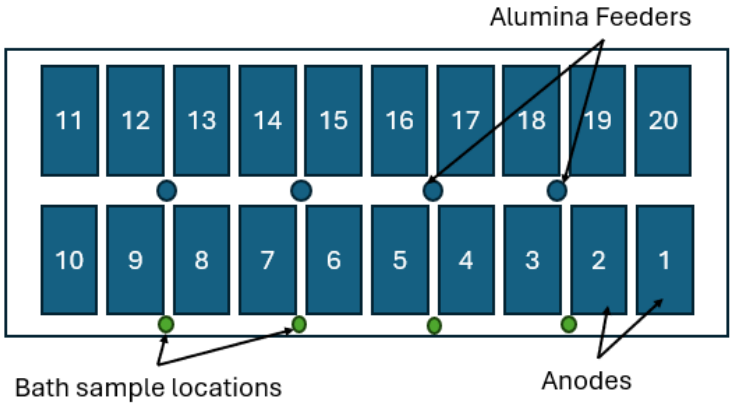

Figure 3. Bath sample locations (4 locations) during the experiment.

Figure 4 and Figure 5 show the recorded line current and individual anode currents during the experiment, respectively. Figure 4 demonstrates that the line current during the experiment was around 272 kA. In Figure 5, anode 5 and anode 6 experienced an anode setting around 5:30, which explains the increasing trend in individual anode currents. It should be noted that the measurement of individual anode current started around 8:50 h and ended around 14:45 h, therefore the spatial alumina estimations were only performed during this period.

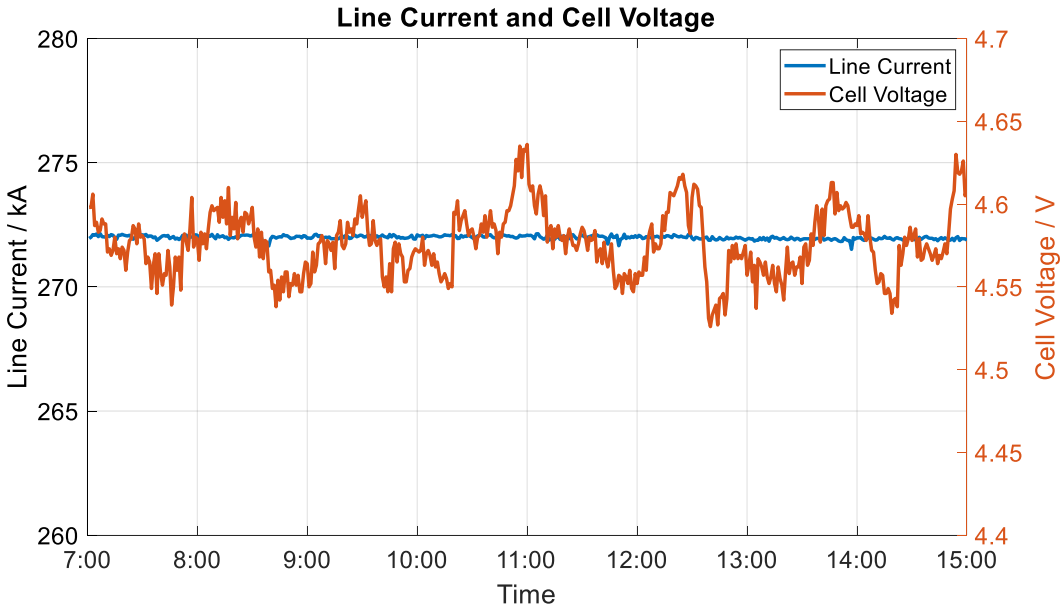

Figure 4. Recorded line current and cell voltage during the experiment.

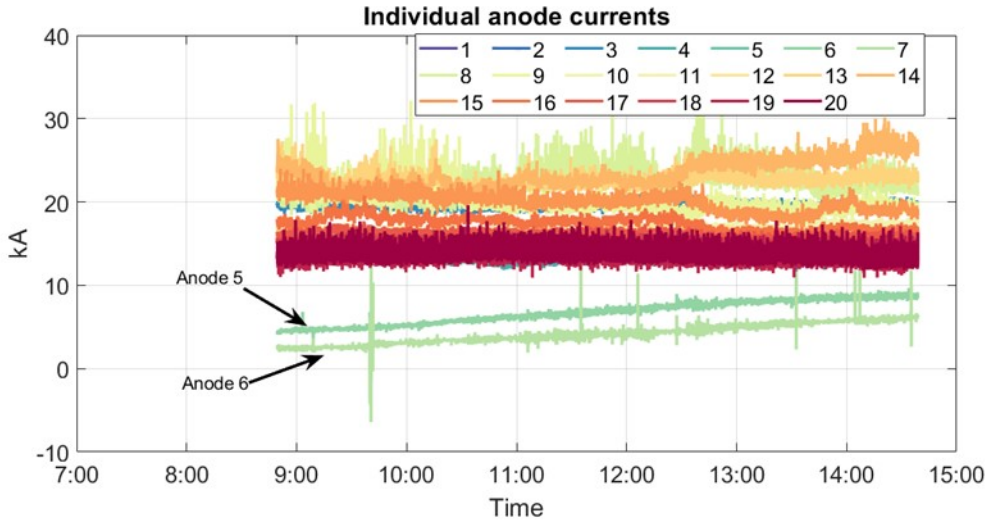

Figure 5. Recorded individual anode currents during the experiment.

Figure 6 and Figure 7 demonstrate the estimated alumina concentration and ACD in Level 1. The alumina feed rate is also plotted to show how it affects the alumina concentration. By analysing the data presented, it can be seen that the estimated alumina concentration aligns well with trend of the measured alumina concentration. The variation in the estimated alumina concentration is primarily affected by the alumina feeding rate. In this experiment, the alumina feeding rate was categorised into four distinct feeding windows: superfast feed, over feed, base feed and under feed. The estimated alumina concentration under varying feeding windows offers valuable insights into the impact of different feeding rates on the overall alumina concentration. Regarding

the estimated ACD, it dropped gradually over time. This decrease is due to the metal accumulation rate being higher than the anode consumption rate. Additionally, the estimated ACD accurately responds to beam movements when they are detected, illustrating its sensitivity to real-time changes in the system.

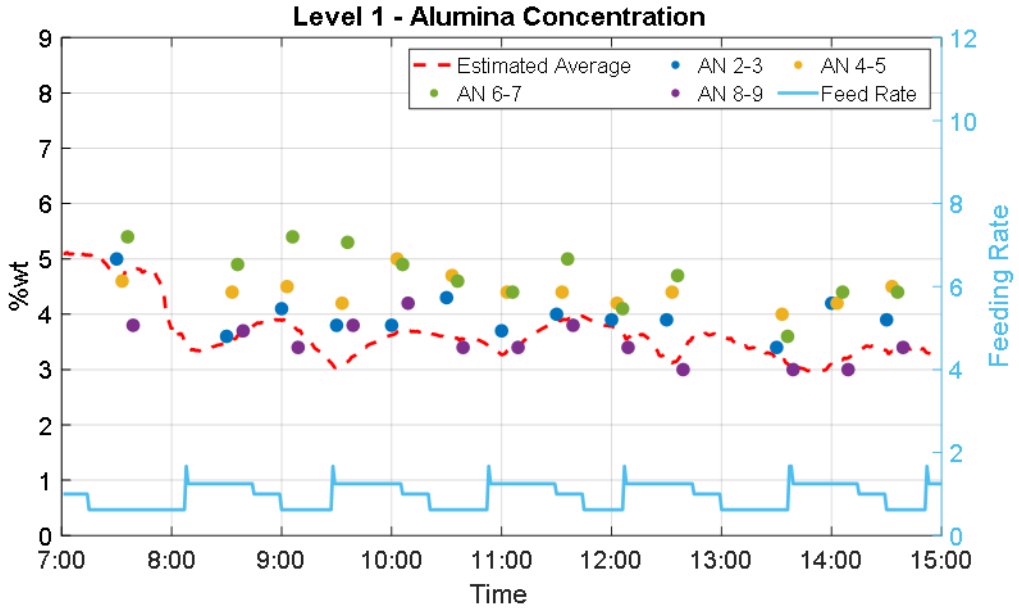

Figure 6. Estimated alumina concentrations, measured alumina concentrations and corresponding feeding rate during the experiment.

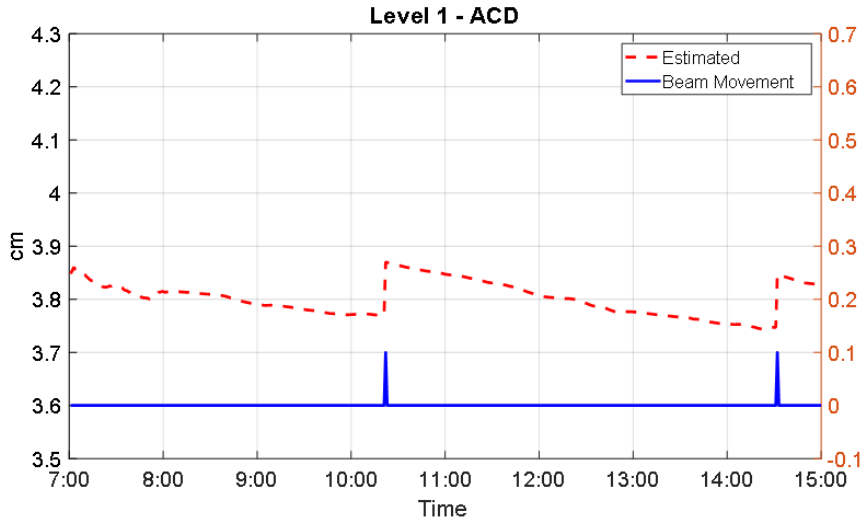

Figure 7. Estimated ACD and recorded beam movements in Level 1.

Figure 8 and Figure 9 demonstrate the estimated alumina concentrations in two different zones and their corresponding ACD in Level 2. It can be seen that the estimated alumina concentration and ACD exhibit different behaviours in different zones. This variation is due to the differences in the distribution of individual anode current, which lead to differences in the alumina consumption rate and the anode consumption between zones.

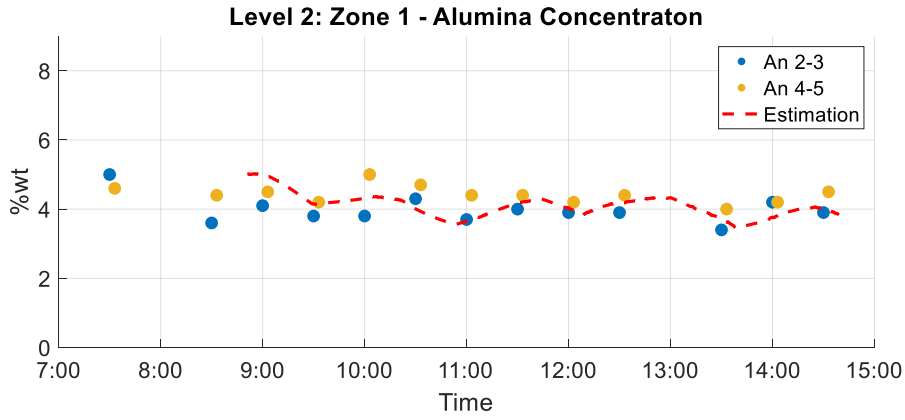

(a) Zone 1

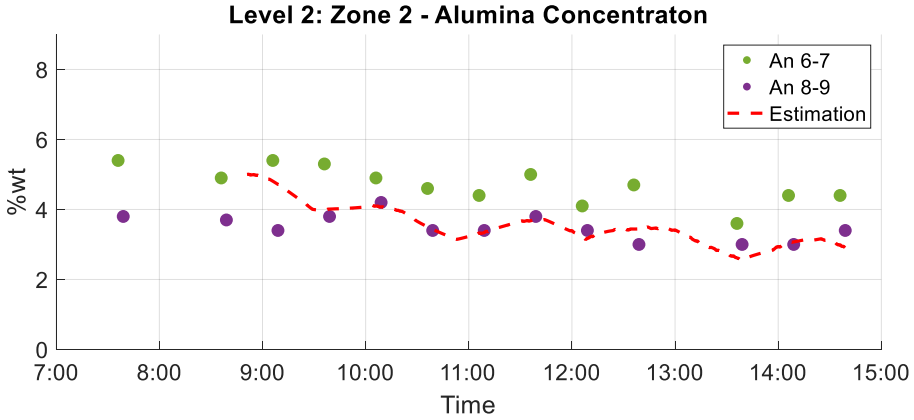

(b) Zone 2

Figure 8. Estimated alumina concentrations and measured alumina concentrations of Zone 1 and Zone 2 in Level 2.

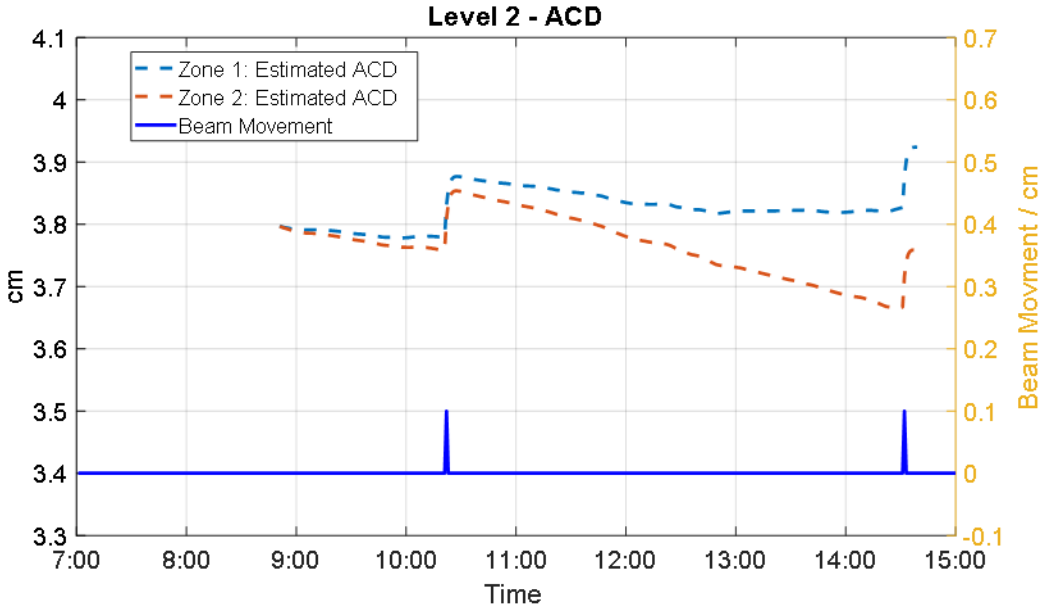

Figure 9. Estimated ACD of Zone 1 and Zone 2 in Level 2.

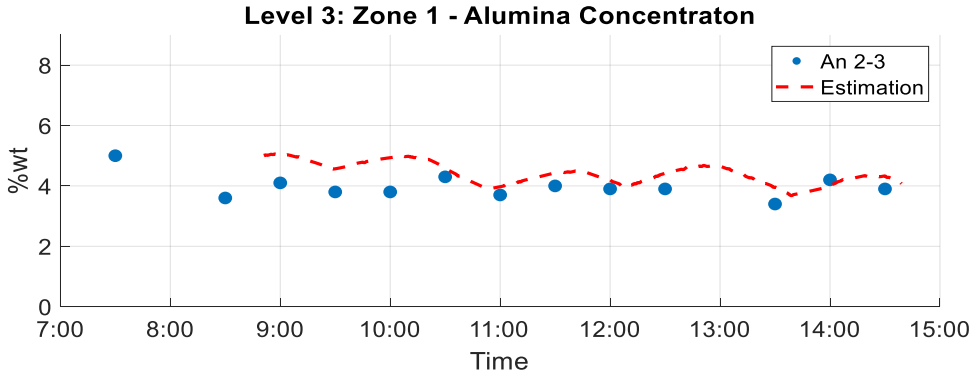

(a) Level 3: Zone 1

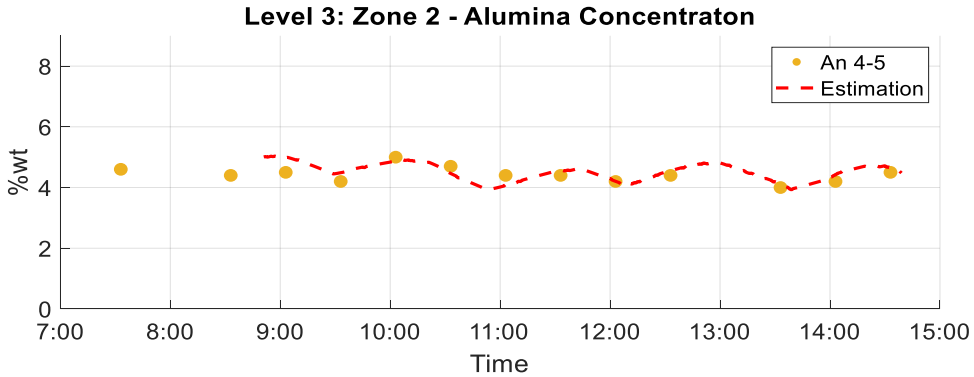

(b) Level 3: Zone 2

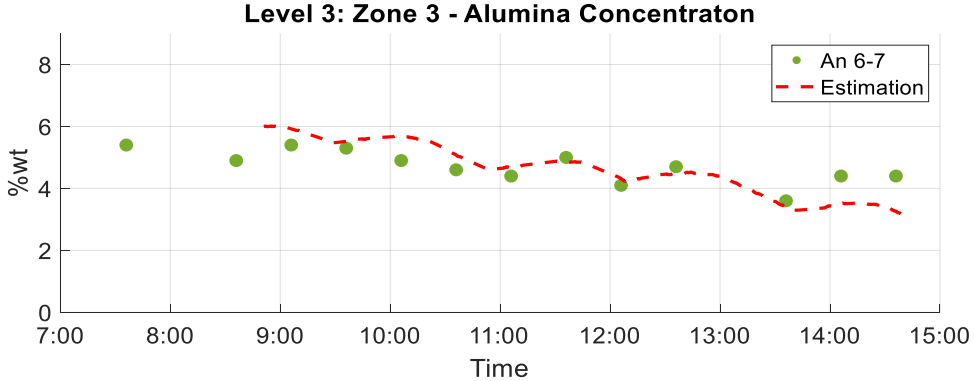

(c) Level 3: Zone 3

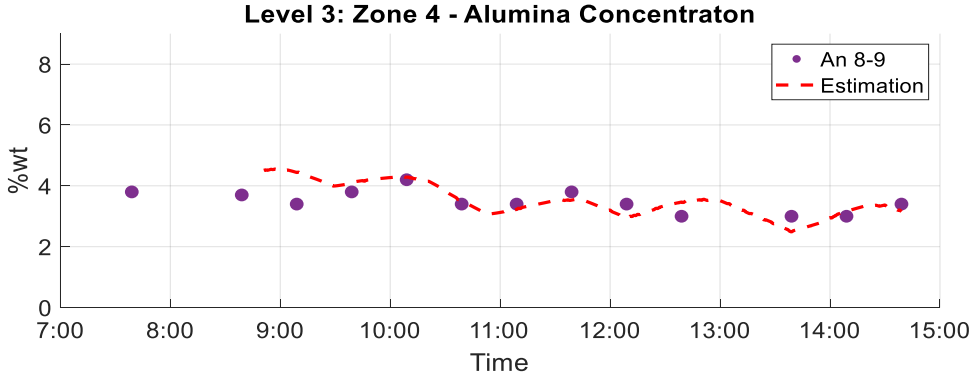

(d) Level 3: Zone 4

Figure 10. Estimated alumina concentrations and measured alumina concentrations of Zone 1, Zone 2, Zone 3 and Zone 4 in Level 3.

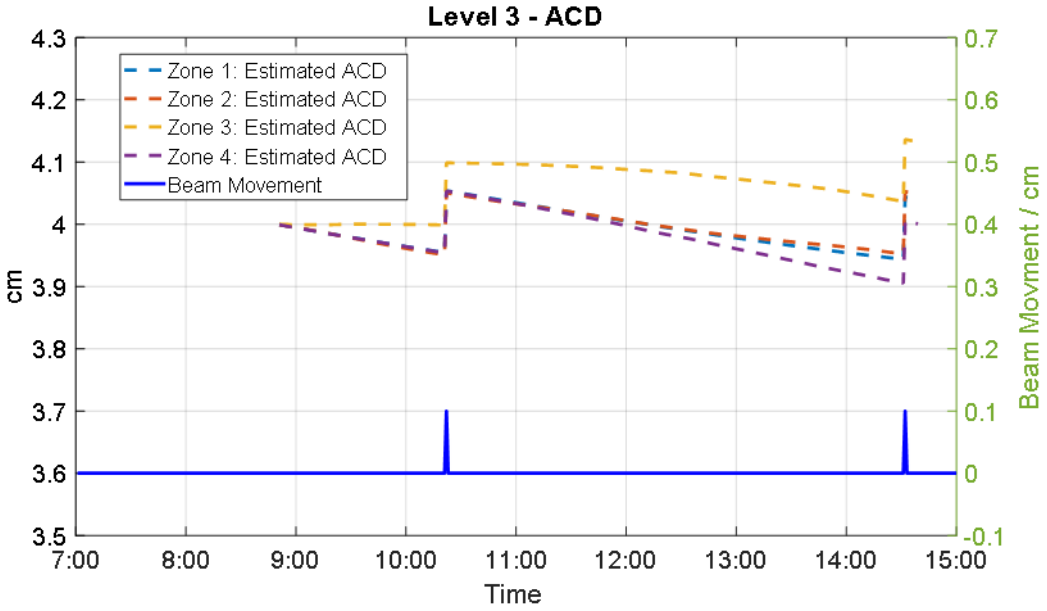

Figure 11 Estimated ACD of Zone 1, Zone 2, Zone 3 and Zone 4 in Level 3.

Figure 10 and Figure 11 demonstrate the estimated spatial alumina concentrations in four different zones and their corresponding ACD in Level 3. By comparing the estimated spatial alumina concentrations with the measured values, it can be seen that the proposed multilevel state observer performs a good alignment in the distribution. Different with the estimation in level 2, the difference in estimated alumina concentrations between zones in Level 3 are affected not only by the distribution of individual anode currents but also by the uneven number of anodes and the uneven bath mass in each zone. Therefore, the experimental results confirm that the multilevel state observer is a reliable tool for monitoring spatial alumina concentrations and providing a reference for localised ACD information in smelting cells.

6. Conclusions

Online monitoring of alumina concentration is important for the improvement of alumina feeding control. Specially, spatial alumina concentration estimation can be used for distributed alumina feeding control to enhance process efficiency and reduce abnormalities. To achieve this, an H_∞ filter-based multilevel state observer is proposed. The application of the H_∞ filter increases the robustness of alumina concentration estimation under different cell conditions, while the multilevel state observer structure enables spatial alumina concentration estimations without requiring detailed bath flow patterns. Experimental results demonstrate the effectiveness of this method. In the future, this multilevel state observer structure can also be applied to spatial thermal estimation.

7. Acknowledgements

The authors wish to acknowledge the financial support from ARC Research Hub for Integrated Energy Storage Solutions (grant number IH180100020), and Emirates Global Aluminium Jebel Ali Operations for their technical support especially from the Technology Development and Transfer team and Operations team.

8. References

1. Yuchen Yao, *Process monitoring, modelling and fault diagnosis in aluminium reduction cells,* PhD Thesis , UNSW Sydney, 2017.
2. Warren Haupin, Halvor Kvande, Thermodynamics of electrochemical reduction of alumina, *Essential Readings in Light Metals: Volume 2 Aluminum Reduction Technology*, 2016, 160-165.
3. Warren Haupin, Principles of aluminum electrolysis, *Essential Readings in Light Metals: Volume 2 Aluminum Reduction Technology* 2016, 3-11.
4. Pierre-Yves Geay, Barry Welch Barry and Pierre Homsi, Sludge in operating aluminium smelting cells, *Essential Readings in Light Metals: Volume 2 Aluminum Reduction Technology*, 2016, 222-228, https://doi.org/10.1007/978-3-319-48156-2_32.
5. Marco A. Stam, et al., Common cell behavior and cell abnormalities in aluminium reduction cells, *Light Metals* 2008, 309-314.
6. Nazatul Aini Abd Majid et al., Detecting abnormalities in aluminium reduction cells based on process events using multi-way principal component analysis (MPCA), *Light Metals* 2009, 589-593.
7. Jing Shi, *Advanced Alumina Feeding Control of Aluminium Smelting Cell*, PhD thesis, UNSW Sydney, 2021.
8. Jing Shi et al. Advanced model-based estimation and control of alumina concentration in an aluminum reduction cell, *JOM*, Volume 74 Jan 2012, 706–717.
9. Jing Shi, et al., Advanced Monitoring and Control of Alumina Concentration in Aluminum Smelting Cells, *IFAC-PapersOnLine* 56.2 (2023): 6194-6199.
10. Yuchen Yao, et al., Monitoring local alumina dissolution in aluminum reduction cells using state estimation. *Light Metals 2015* (2016), 577-581.
11. Dan Simon, *Optimal state estimation: Kalman, H infinity, and nonlinear approaches*. John Wiley & Sons, 2006.
12. Vidya S.Rao, George V.I and Surekha Kamath, Comparison of Kalman observer and H infinity observer designed for TRMS, *International Journal of Control and Automation*, 9.10 (2016), 275-292.
13. Héctor Poveda et al., Kalman vs H∞ filter in terms of convergence and accuracy: Application to carrier frequency offset estimation, *2012 Proceedings of the 20th European Signal Processing Conference (EUSIPCO)*, IEEE, 2012.
14. Luning Ma et al., Estimation of the Spatial Alumina Concentration of an Aluminium Smelting Cell Using a Huber Function-Based Kalman Filter, *Lighty Metals* 2024, 464-473.
15. Yuchen Yao et al. Estimation of spatial alumina concentration in an aluminum reduction cell using a multilevel state observer, *AIChE Journal*, 63.7 (2017), 2806-2818.